ADVANCED MATERIALS INTERFACES
www.advmatinterfaces.de

PEDOTS:PSS@KNF Wire-Shaped Electrodes for Textile Symmetrical Capacitor

*Eugenio Gibertini and Luca Magagnin**

The emerging wearable electronics and e-textiles have motivated tremendous interests in textile energy storage microdevices. Among them, fiber-shaped capacitors (FSCs) offer unique properties because of their 1D configuration and reliable energy storage. In recent years, many works focused on the development of 1D fibrous-shaped electrodes usually involving complex material synthesis and techniques. Herein, an easy procedure for the preparation of composite fibers made by PEDOT:PSS infiltration in gel-state Kevlar nanofiber (KNF) wires is proposed. The PEDOT:PSS@KNF 1D electrodes are mechanically robust, conductive, and flexible. The symmetric FSCs integrated in textile show remarkable capacitance retention under deformation, average capacitance of 1.1 mF, volumetric energy density of 71 mWh cm^{-3}, and ability to power on a blue light-emitting diode.

1. Introduction

In the last years, smart fabrics and e-textiles gained tremendous interest both in research community and industry. In fact, embedding flexible, comfortable, and lightweight microdevices in our clothes could represent a technological breakthrough and will certainly push the diffusion of wearable electronics in our every-day life.[1–3] Recently, great efforts have been paid to the development of adequately miniaturized and textile-integrated electronics such as communication system,[4–6] luminescent,[7,8] and multi-purpose sensors.[9–15] However, these microdevices should be powered on and actuated by embedded energy storage and power sources and fibrous-shaped electrodes are particularly promising because of their 1D configuration that offers unique advantages of flexibility and wearability that cannot be fulfilled by conventional 2D planar device architecture. Both fiber-shaped capacitors (FSCs) and batteries have been recently developed but the environmental susceptibility of the latter as well as their employment of toxic organic electrolyte is always a matter of concerns.[16] On the contrary, FSCs could represent a more reliable, safer, and longer lifecycle alternative. A number of fibers made of graphene, carbon nanotubes, conductive polymer and, more recently, MXenes were successfully obtained by wet-spinning technique and investigated as 1D electrodes for wearable supercapacitors.[17–29] However, these materials usually involve complex procedure for their synthesis, harmful dispersant solvent or post-treatment steps to produce fibers with sufficient mechanical resistance and electrochemical performances. Aramid nanofibers (ANFs) have been recently proposed as a new nanoscale building block to design new composite materials.[30] Contrary to standard route based on monomer polymerization, ANFs can be easily and quickly obtained through top-down approach by dissolution of aramid polymeric chains and then re-assembled in macroscopic fibers or film by solution processing.[30,31] Aramid polymer is well-known for its mechanical strength but it's not electrically conductive and must be loaded with conductive fillers to achieve electronic transport. Up to date, ANFs have been mainly investigated as filler for polymers reinforcement,[32,33] matrix for multi-purpose membranes,[34–37] thermal shields,[38,39] and even additive for separators and solid-state electrolyte for Li-ion batteries.[40,41] However, despite the good wet-spinnability of KNF dispersions, only poor attention was paid to the employment of ANFs for making FSCs. In previous work, Cao et al. fabricated fibers with core–shell structure by co wet-spinning a core carbon nanotube dispersion and a sheath ANFs dispersion.[42] The symmetrical FSCs obtained by infiltration with H_3PO_4/PVA gel electrolyte showed a remarkable linear capacity up to 0.75 mF cm^{-1}. Wang et al. loaded graphene nanoplatelets (GNPs) to a ANF dispersion to obtain a ANFs/GNPs composite wire-shaped electrodes by coagulation in a water/acetic acid solution.[43] However, their results showed that GNPs interfered with the ANFs coagulation by hydrogen bonds restoration between terephthalamide units resulting in a consistent decrease of the tensile strength at high GNPs incorporation in the ANFs matrix.

In this work, PEDOT:PSS@KNFs composite fibers were produced by a simple two-step process involving the nanofibrillation of Kevlar to Kevlar nanofibers (KNF), wet-spinning of the KNF fiber and the following soaking into a PEDOT:PSS aqueous dispersion. In this way, electrically conductive fibers were obtained due to the conductive PEDOT:PSS chains percolation keeping almost unaltered the mechanical resistance of the KNF matrix. The PEDOT:PSS@KNF fibers were flexible, knittable and sewable, and by coupling adjacent two fibers, a symmetric FSC could

E. Gibertini, L. Magagnin
Dipartimento di Chimica
Materiali e Ingegneria Chimica "Giulio Natta"
Politecnico di Milano, Via Mancinelli, 7, Milano 20131, Italy
E-mail: luca.magagnin@polimi.it

The ORCID identification number(s) for the author(s) of this article can be found under https://doi.org/10.1002/admi.202200513.

DOI: 10.1002/admi.202200513

be obtained. The electrochemical tests with a H_3PO_4/PVA gel electrolyte revealed good capacitance retention under deformation and long lifecycle up to 10k cycles. Noteworthy, at the best of our knowledge, FSCs obtained by infiltrating PEDOT:PSS into KNF matrix have not been reported yet.

2. Results and Discussion

2.1. PEDOT:PSS@KNF Fiber

2.1.1. Synthesis

Aramid fibers are aromatic polyamides widely known under their commercial name as Kevlar, Nomex, and Twaron. Aramid polymer is precisely poly p-phenylene terephthalamide (PPTA), which is characterized by highly oriented polymeric chain along the fiber axis that results in a higher amount of chemical bonds between chains. Aligned chains interact each other via strong hydrogen-bonds between carbonyl groups and NH centers of adjacent chains and additional strength is derived from aromatic stacking interactions.[44] ANF can be obtained by a top-down approach[30] involving a "molecular scissoring" taking place in DMSO/KOH solvent system, able to abstract the mobile hydrogen from the amide groups, generating negatively charged PPTA chains and splitting macroscopic fibers to AFN.[30,34] As result, a stable reddish dispersion was obtained (Figure S1, Supporting Information). Both Raman analysis and AFM confirmed successful ANF synthesis (Figures S2 and S3, Supporting Information). **Figure 1** schematically shows the KNF wet spinning and KNF@PEDOT:PSS fibers preparation, while real pictures are provided in Figure S4, Supporting Information. As the KNF dope was extruded in the coagulation bath, solvent exchange occurred by DMSO replacement with EtOH/H_2O and re-protonation of amide groups of PPTA chains took place, restoring the assembly of individual KNF into macroscopic porous structure of aligned fibers. The gel-state KNF fibers were soaked in the diluted PEDOT:PSS dispersion and finally dried to obtain PEDOT:PSS@KNF. After immersion, the typical yellow color of KNF fiber turned dark blue. DMSO was added in the PEDOT:PSS dispersion as conductivity enhancer additive. In fact, it has been widely reported that additives as cosolvents, acids, or surfactants greatly enhance PEDOT:PSS conductivity and DMSO has been proved as one of the most performing conductivity tuning agent.[45–49] Multi-yarns fibers could also be prepared by twisting up to four single yarns PEDOT:PSS@KNF (Figure S5, Supporting Information). However, the manual twisting resulted in poor control on the process and final repeatability of the electrode performances. As consequence, only single-wire electrodes were considered in the work.

2.1.2. Characterization

The PEDOT:PSS loading in the KNF matrix respect to immersion time was monitored by Raman analysis, whose spectra are reported in **Figure 2**. Neat KNF fiber showed the typical PPTA fingerprint with the intense peak at 1608 cm^{-1} and minor peaks at 1273 and 1510 cm^{-1} attributed to the ring C=C stretching mode and C-H bending at 1510 cm^{-1}. The N-H peak was well visible at 1568 cm^{-1}, as symptomatic of the PPTA chains rearrangement through hydrogen bond restoration. By immersion of the KNF fiber in the PEDOT:PSS dispersion, a new peak raised at ≈1440 cm^{-1} as fingerprint of the C_α=C_β symmetric stretching of the five-carbon atoms constitutive of PEDOT ring.[50,51] Likely, the thiophene ring was in the quinoid (C_β=C_β–C_α) conformation, that is, linear or expanded-coil conformation structure, rather than the benzoid one (C_β–C_β=C_α) that is the preferred structure of the undoped and coiled PEDOT:PSS conformation.[50] Noteworthy, the intensity ratio I_P/I_{KNF}, determined as the height (i.e., intensity) ratio, between the C_α–C_β peak of PEDOT:PSS and the C=C of the phenylene ring of KNF increased with the immersion time, passing from 0.6 to 0.89 and 1.05 after 10 min, 1 h, and 12 h of immersion respectively. The I_P/I_{KNF} raise could be attributed to both better coverage and uniform coating on KNF surface by PEDOT:PSS and to higher loading of PEDOT:PSS in the PEDOT:PSS@KNF fibers because of the PEDOT:PSS infiltration toward fiber core.

When the PEDOT:PSS loaded KNF fibers were used as a conductive wires, the *I-V* curves (**Figure 3**a) clearly show that the electrical resistance decreased by immersion time increasing, as consequence of higher PEDOT:PSS loading, better coverage uniformity and improved percolation pattern. In fact, the correspondent conductivity (Figure 3b) increased from 380 to 3097 and 4265 S m^{-1} after 10 min, 1 h, and 12 h of immersion respectively. A fundamental requirement of wearable electronics is the working under deformation and as consequence the conductivity retention, expressed as the R/R_0 ratio (Figure 3c), was evaluated by measuring the resistance value upon 400 bending cycles (180°). The average R/R_0 was 1.015 ± 0.04, meaning that the PEDOT:PSS@KNF fiber was not damaged and the KNF matrix provide sufficient mechanical resistance to avoid cracking of the fragile PEDOT:PSS. In Figure 3d, the specific conductivity value at 12 h immersion time is compared to those of reference works where PEDOT:PSS-based fibers were

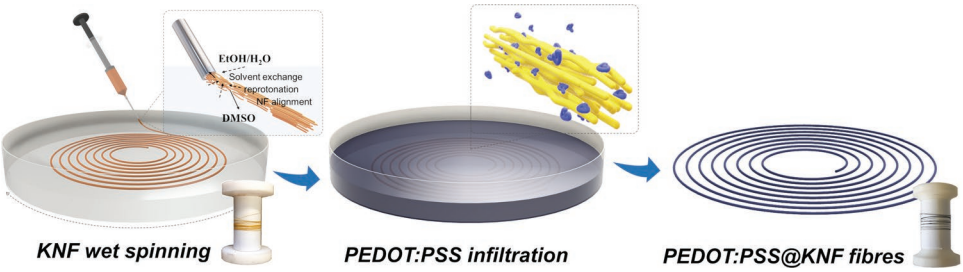

Figure 1. Schematic illustration of the process leading to PEDOT:PSS@KNF fiber synthesis.

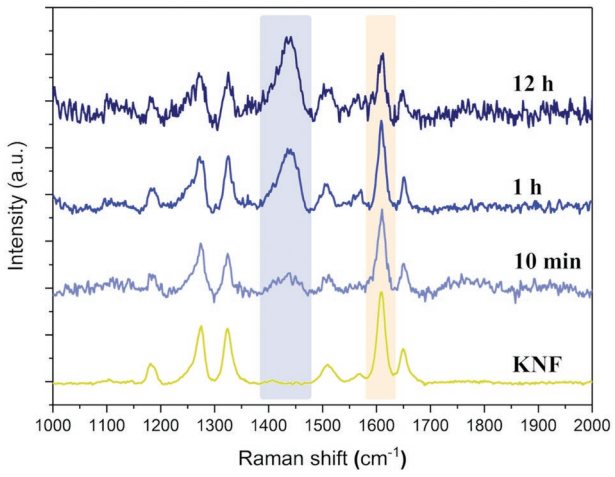

Figure 2. Raman spectra for the KNF and PEDOT:PSS@KNF at different immersion time. The light blue and yellow rectangles highlight the fingerprint peaks associated to PEDOT:PSS and KNF, respectively.

obtained by wet-spinning, such as PEDOT:PSS blended with PU,[20] PVA,[52,53] PAN[54] and neat PEDOT:PSS.[26,55–60] Our PEDOT:PSS@KNF fiber showed specific conductivity up to two orders of magnitude lower respect to neat PEDOT:PSS fibers but among the highest values for the PEDOT:PSS/polymer composite fibers.

The mechanical properties of both KNF and PEDOT:PSS@KNF fibers were evaluated through tensile stress test. **Figure 4**a shows that both the ultimate tensile strength and elongation break of KNF and PEDOT:PSS@KNF fibers were comparable and demonstrated that by our two-step process mechanical properties of KNF were unaltered because the restoration of the strong PPTA chains macrostructure was not hindered nor obstructed. The ultimate tensile strength, elongation break, and Young Modulus, measured on five samples average, were 139.58 MPa, 10.08% and 63.36 MPa for the KNF fibers and 146.72 MPa, 9.45%, and 74.24 MPa for the PEDOT:PSS@KNF respectively (Figure 4b). Although the values were very similar, a slight increase in the mechanical properties resulted from

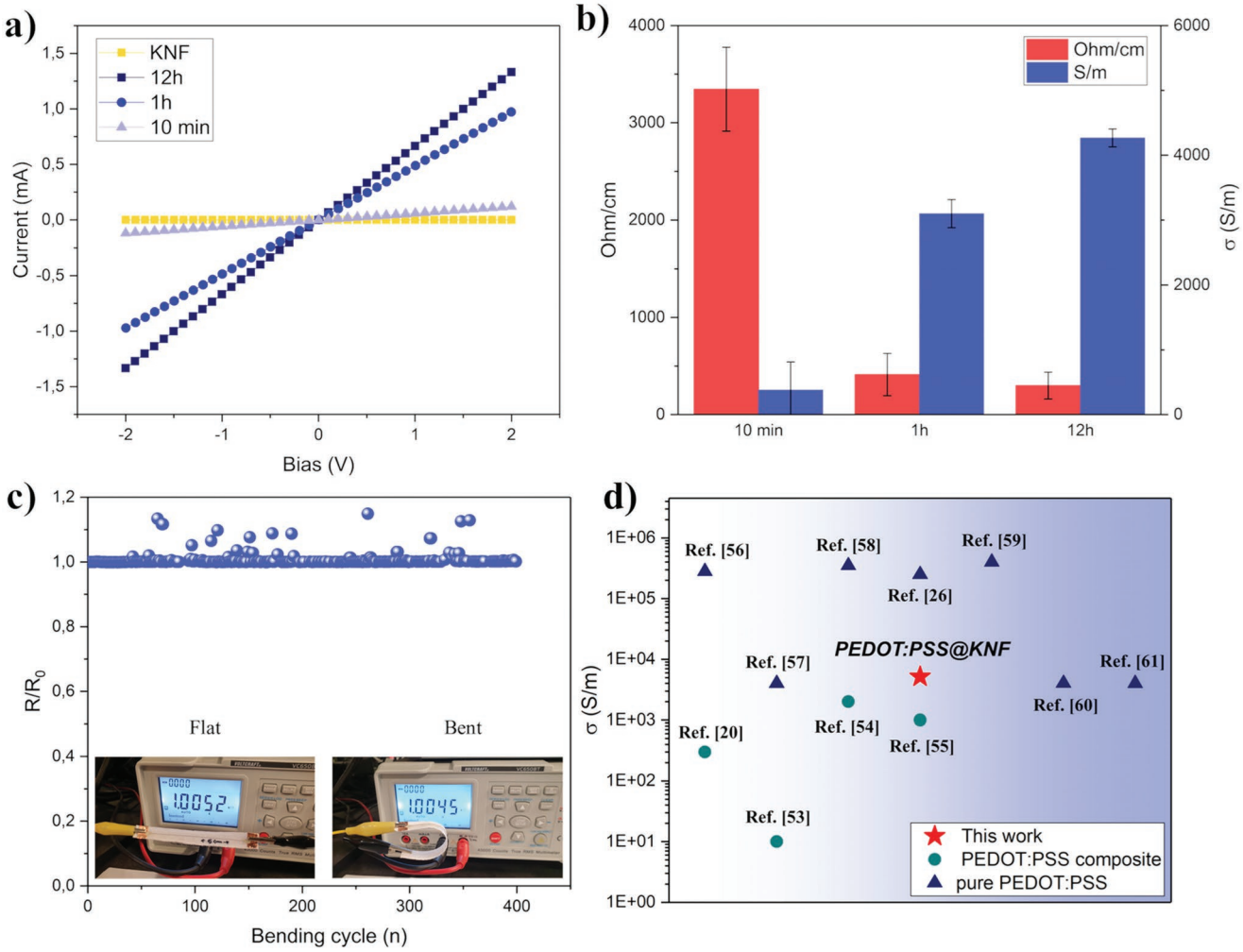

Figure 3. *I–V* curve of the PEDOT:PSS@KNF samples (a), specific resistance and conductivity (b), and resistance retention on 400 bending cycles (c). In (d), the comparison of the specific conductivity values for the 12 h immersion PEDOT:PSS@KNF sample respect to similar literature works is shown.

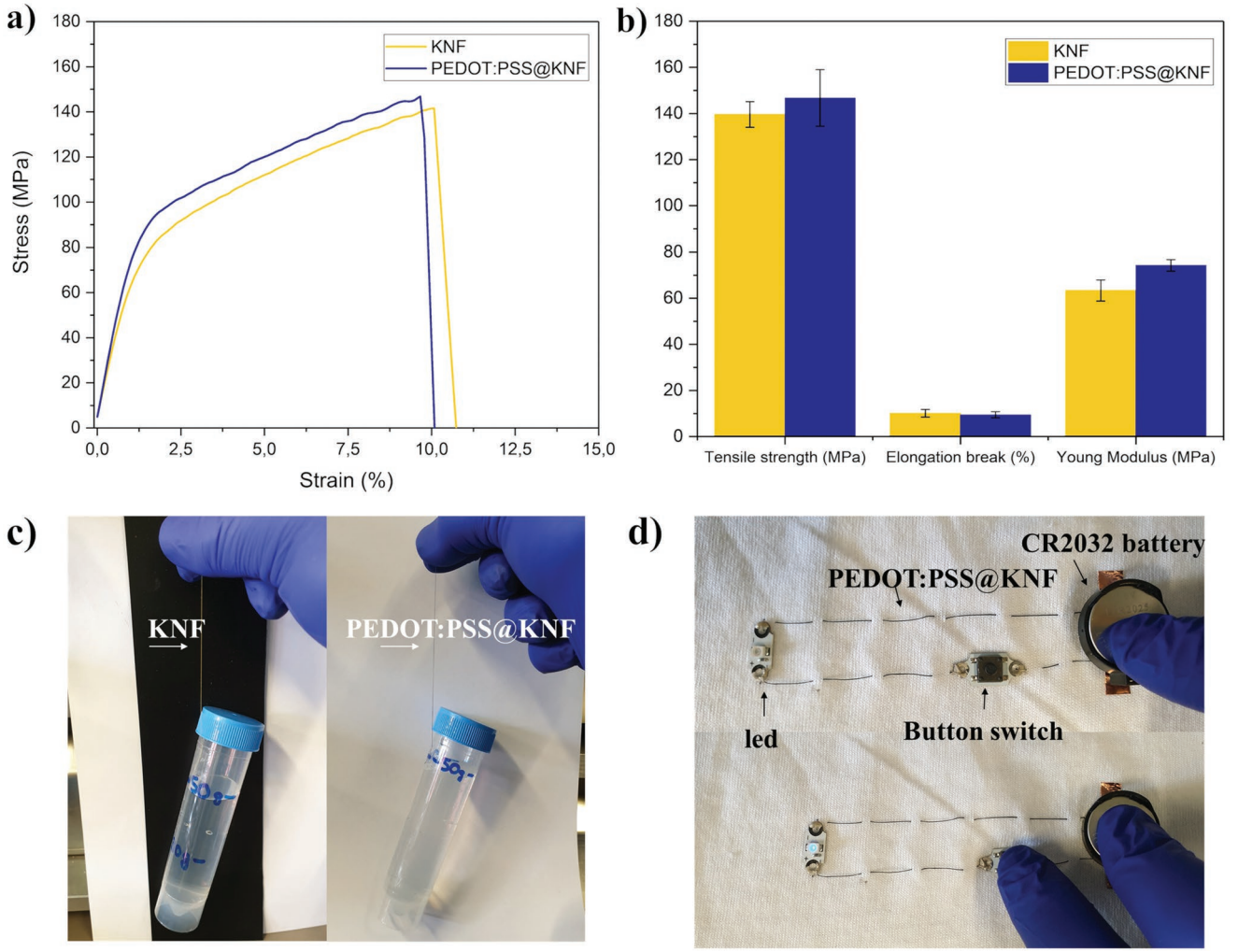

Figure 4. Tensile stress–strain curve (a) and summary of the main mechanical properties of the KNF and PEDOT:PSS@KNF fibers (b). The thin fibers were able to sustain the weight of a tube filled with 50 g of H_2O (c) and combined enough mechanical strength, flexibility, and electrical conductivity to be hand-sewed and integrated into electrical circuit (d).

PEDOT:PSS infiltration because of the uniform polymeric PEDOT:PSS matrix formation after complete solvent evaporation. However, it is noteworthy to mention that mechanical properties are strongly influenced by process parameters and fiber post-treatment but in this work a proper optimization of processing to tune the mechanical properties was neglected. Moreover, ultimate tensile strength of $\approx 10^2$ MPa and elongation break ≈10% are typical values for KNF-based wet-spinned fibers.[33,42,43,61] The PEDOT:PSS@KNF fiber was flexible and strong enough to sustain a 50 g weight (Figure 4c) and to be hand-sewed (Figure 4d) to a cotton textile to produce an electronic circuit capable of transporting the current to a blue led.

The KNF fiber (**Figure 5**a) showed a rather smooth morphology and preferential orientation of KNFs along the axial direction was visible (Figure 5b) as result of the KNFs alignment by the shear force of the rotating coagulation bath. The surface of PEDOT:PSS@KNF fiber was corrugated because of the PEDOT:PSS coating (Figure 5c) and the preferential alignment direction was even more visible. The fiber surface became much rougher and more wrinkled respect to the neat KNF fiber (Figure 5d,e) and it could be highlighted that the PEDOT:PSS wrinkles were well aligned along the fiber direction, showing that both the re-assembled ANF and PEDOT:PSS clusters were anisotropically orientated. The morphology resembled exactly similar literature work.[59] Few cracks were also visible and may be attributed to the inhomogeneous evaporation of the solvent, faster on the surface where a crosslinked PEDOT:PSS skin was quickly formed and slower from the fiber core. Remarkably, PEDOT:PSS@KNF flexibility was demonstrated by its knotting ability (Figure 5f). Sulfur was chosen as target element in EDS mapping analysis to assess both the uniformity on surface and penetration depth of the PEDOT:PSS in the fiber core, as sulfur from the PSS pendant groups was not present in the PPTA chains. The signal from sulfur was homogeneous from fiber surface (Figure 5g) revealing a defect-free coating layer. More interestingly, the S signal distribution from the sample cross-section (Figure 5h) indicated that PEDOT:PSS particles in suspension, driven by concentration gradient, were able to diffuse

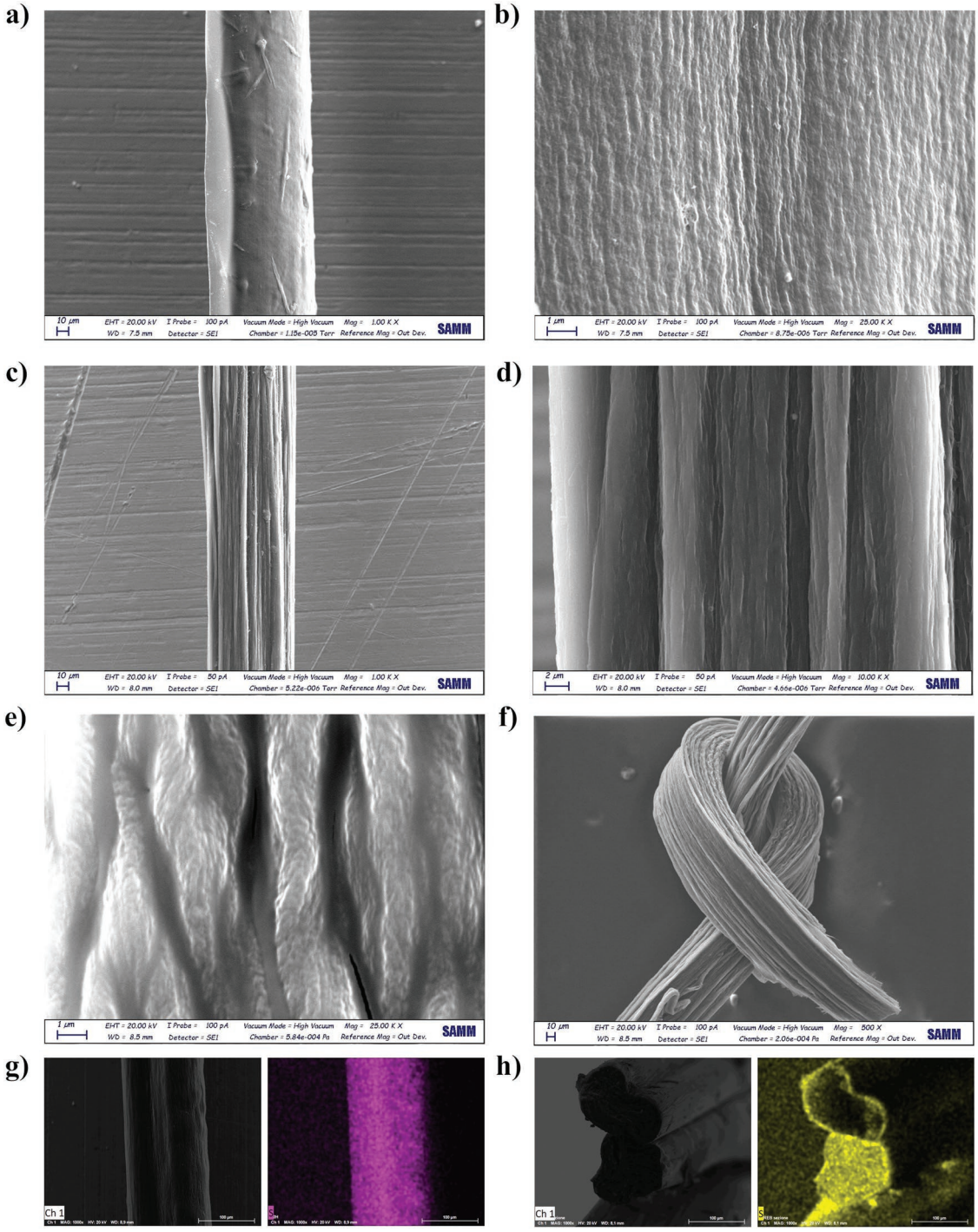

Figure 5. SEM images of the KNF (a,b) and PEDOT:PSS@KNF fibers (c–f) at different magnification. In (g,h), the elemental maps of sulfur from the PEDOT:PSS@KNF surface and cross-section are reported.

and penetrate to the inner core of the KNF gel state fiber and not simply coating the fiber surface. In summary, EDS analysis of the fiber cross-section revealed the formation of a composite PEDOT:PSS@KNF fiber, without evidence of chemical bonds formation, in which a PEDOT:PSS conductive matrix interpenetrated the one of the previously formed KNF macroscopic fiber.

2.2. PEDOT:PSS@KNF FSC

2.2.1. Single Electrode Electrochemical Characterization

PEDOT:PSS@KNF were tested as fiber-shaped capacitor (FSC) in 1 M H_3PO_4 solution. **Figure 6**a shows that limiting the anodic potential at +0.6 V versus SCE, the corresponding cyclic

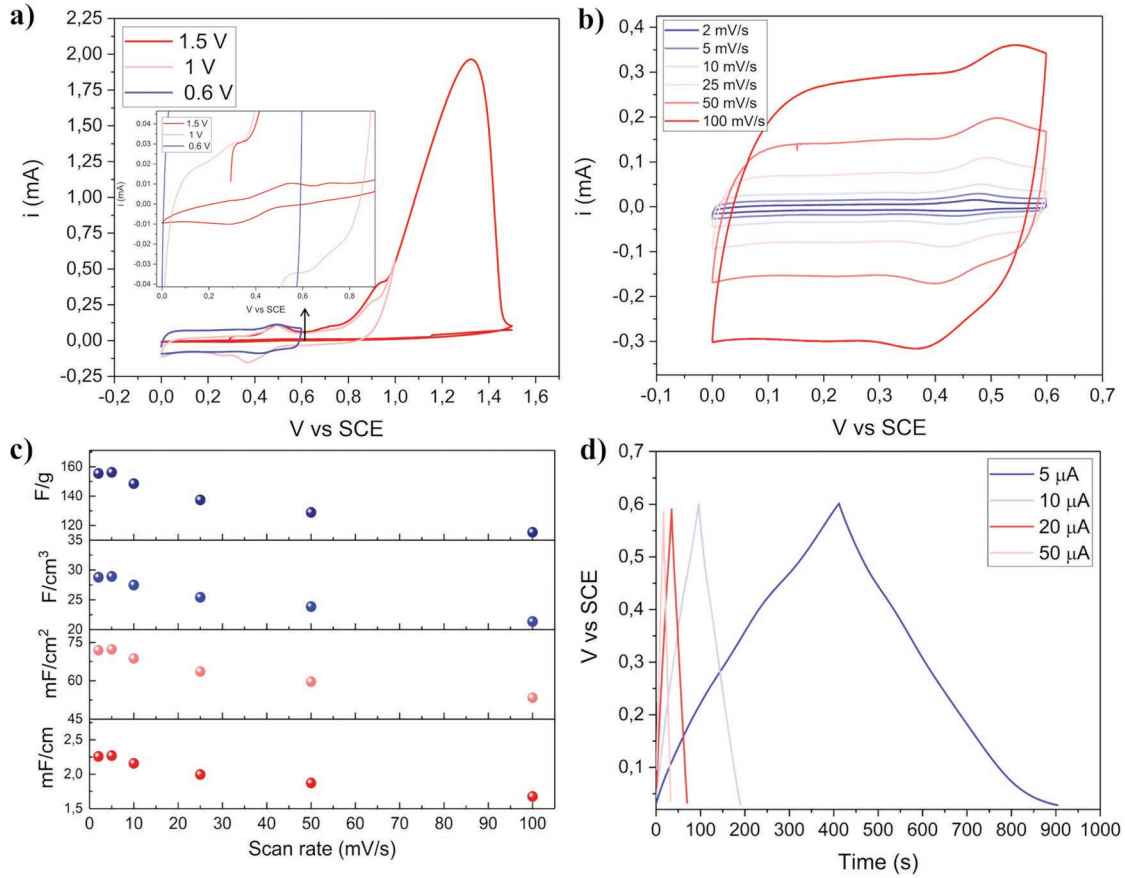

Figure 6. a) Cyclic voltammetries at increasing anodic potential limit at 25 mV s^{-1}. Cyclic voltammetries at increasing scan rate (b) for the PEDOT:PSS@KNF electrode immersed in 1 M H_3PO_4 electrolyte and corresponding values of linear capacitance (mF cm^{-1}), areal capacitance (mF cm^{-2}), volumetric capacitance (F cm^{-3}), and specific capacitance (F g^{-1}) (c). The typical electrode length is ≈3 cm and mass 0.13 mg cm^{-1}. In (d), the galvanostatic charge/discharge voltage profiles at different currents are reported.

voltammetry was almost perfectly rectangular while extending it a +1 V versus SCE and, more evidently, at +1.5 V versus SCE irreversible over-oxidation took place. Beyond 1 V versus SCE a broad anodic peak was present related to the irreversible PEDOT:PSS over-oxidation and confirmed by the absence of the corresponding cathodic peak at the reverse scan and loss of conductivity at the successive cycle. PEDOT:PSS over-oxidation has been investigated and demonstrated by previous studies that revealed irreversible decrease in the conjugation length of the polymer's delocalized π-bond, through cross-linking of the polymer chains, and loss of conductivity.[62,63] For these reasons, the electrochemical potential window was limited to 0.6 V versus SCE. The cyclic voltammetries (Figure 6b) appeared rectangular even at high scan rate with a couple of reversible anodic and cathodic peaks rising respectively at around 0.43 and 0.47 V versus SCE. As other conductive polymers PEDOT:PSS is considered to have mainly double-layer capacitance that originates from the electrical double layers formed along the nano-scaled interfaces between PEDOT-rich and PSS-rich grains that comprise two phases of the bulk of PEDOT:PSS.[64] However, in acidic electrolyte or in the presence of cations in solution, a pseudo-capacitive storage may arise according to the equation:[65,66]

$$PEDOT^+:PSS^- + M^+ + e^- \leftrightarrow PEDOT^0 + M^+:PSS^- \quad (1)$$

where M^+ is a metal cation or H^+. The capacitance values normalized on length (mF cm^{-1}), area (mF cm^{-2}), volume (F cm^{-3}), and electrode mass (F g^{-1}) are given in Figure 6c while the detailed values are reported in Table S1, Supporting Information. The linear capacitance ranged from 2.26 mF cm^{-1} (10 mV s^{-1}) to 1.68 mF cm^{-1} at 10 mV s^{-1} and the specific capacitance is in the order of 10^2 F g^{-1}, as typical for supercapacitors. Moreover, PEDOT:PSS@KNF fiber-shaped electrode showed remarkable rate capability, retaining the 74.2% of the capacitance even at the highest scan rate. The galvanostatic charge and discharge test (Figure 6d) showed the typical triangular-shape profile of double-layer capacitors. The linear capacitance was 1.24 mF cm^{-1} when a current of 1.6 µA cm^{-1} was applied, decreasing to 0.86 mF cm^{-1} by increasing discharge current to 16.6 µA cm^{-1}.

2.2.2. PEDOT:PSS@KNF Textile Symmetrical Capacitor

The rectangular shape of the cyclic voltammetry in the selected potential window allows to build symmetrical capacitors with the reasonable assumption that the potential is equally distributed on the two equal electrodes. The symmetrical FSCs were obtained by placing two or more electrodes parallelly close to

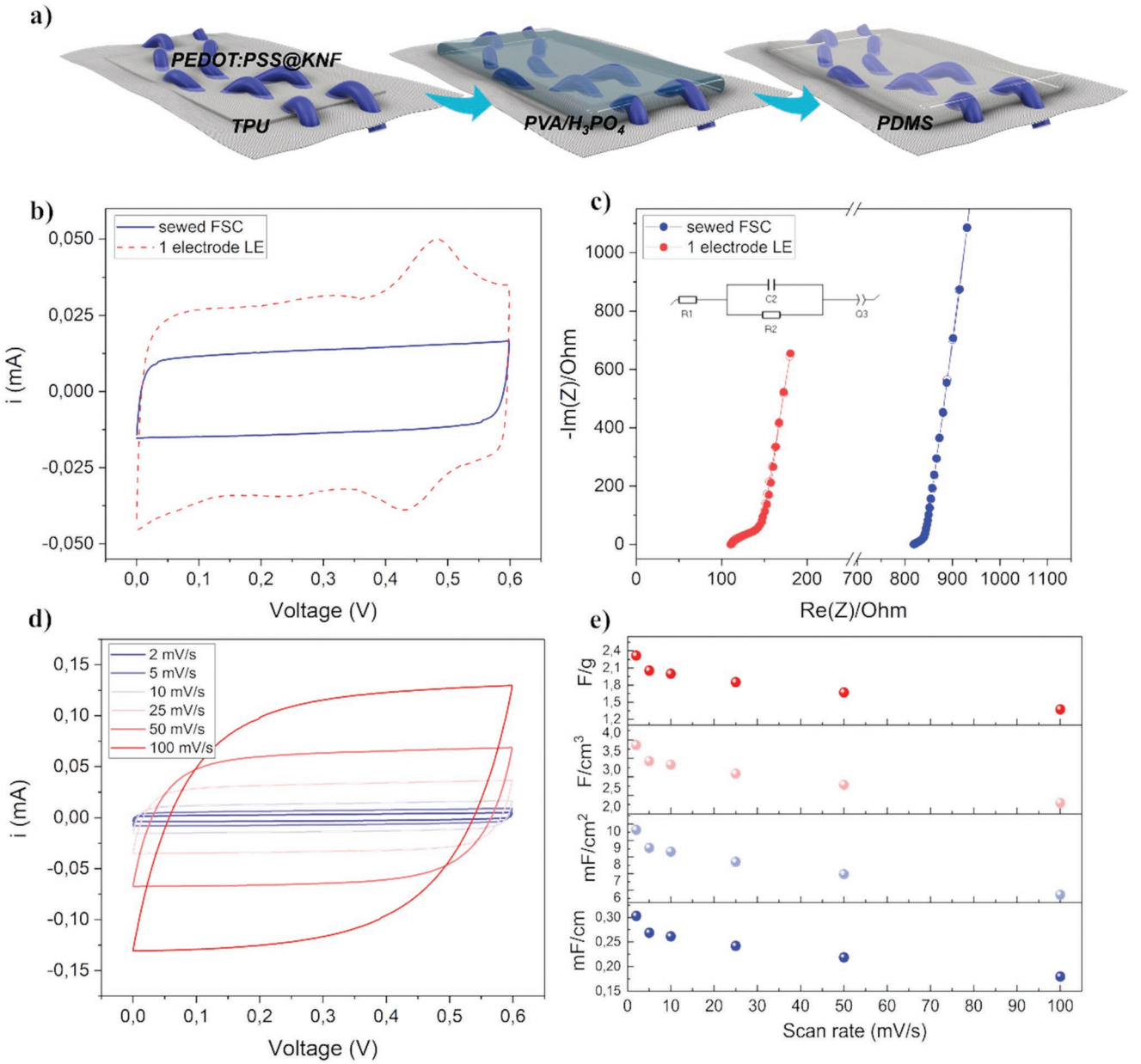

Figure 7. a) Schematic drawing of the FSCs produced by hand-sewing the PEDOT:PSS@KNF electrodes to the fabric substrate. The cotton fabric was covered with a thin thermoplastic TPU sheet to insulate the FSC and electrolyte from the bottom side. After PEDOT:PSS@KNF integration, the H_3PO_4/PVA gel was casted and dried and PDMS coating was then casted on top for final sealing. Cyclic voltammetry comparison at 10 mV s^{-1} (b) for the symmetric hand-sewed FSC compared to the single PEDOT:PSS@KNF electrode in liquid electrolyte solution (LE). c) Nyquist plots of the FSC, with the fitting model displayed in inset figure. In (d,e), the CVs at different scan rate and the corresponding values of normalized capacitance are given for the sewed FSC.

each other on textile and covering them with the semi-solid H_3PO_4/PVA electrolyte and PDMS for final sealing (**Figure 7**a).

The cyclic voltammetry was almost perfectly rectangular (Figure 7b) confirming that a symmetrical FSC can be produced with the PEDOT:PSS@KNF electrodes. Moreover, hand-sewing was compared to fixing the fiber-shaped electrodes with bi-adhesive tape on fabric surface (Figure S6, Supporting Information) since sewing could eventually induce damages in the PEDOT:PSS@KNF because of the folding and knotting of the PEDOT:PSS@KNF electrodes. However, the two CVs were almost overlapping (Figure S7, Supporting Information) demonstrating our fiber-shaped electrodes were flexible and mechanically strong enough to be hand-sewed without degrading the electrochemical performances. However, comparing it with the CV of the single PEDOT:PSS@KNF (Figure 7b) the lower current can be mainly ascribed to the difference in conductivity between the liquid H_3PO_4 solution and the semi-solid H_3PO_4/PVA gel. In fact the equivalent series resistance that is the sum of electrolyte and electrode internal resistance, shifted on the real axis of the Nyquist plot from

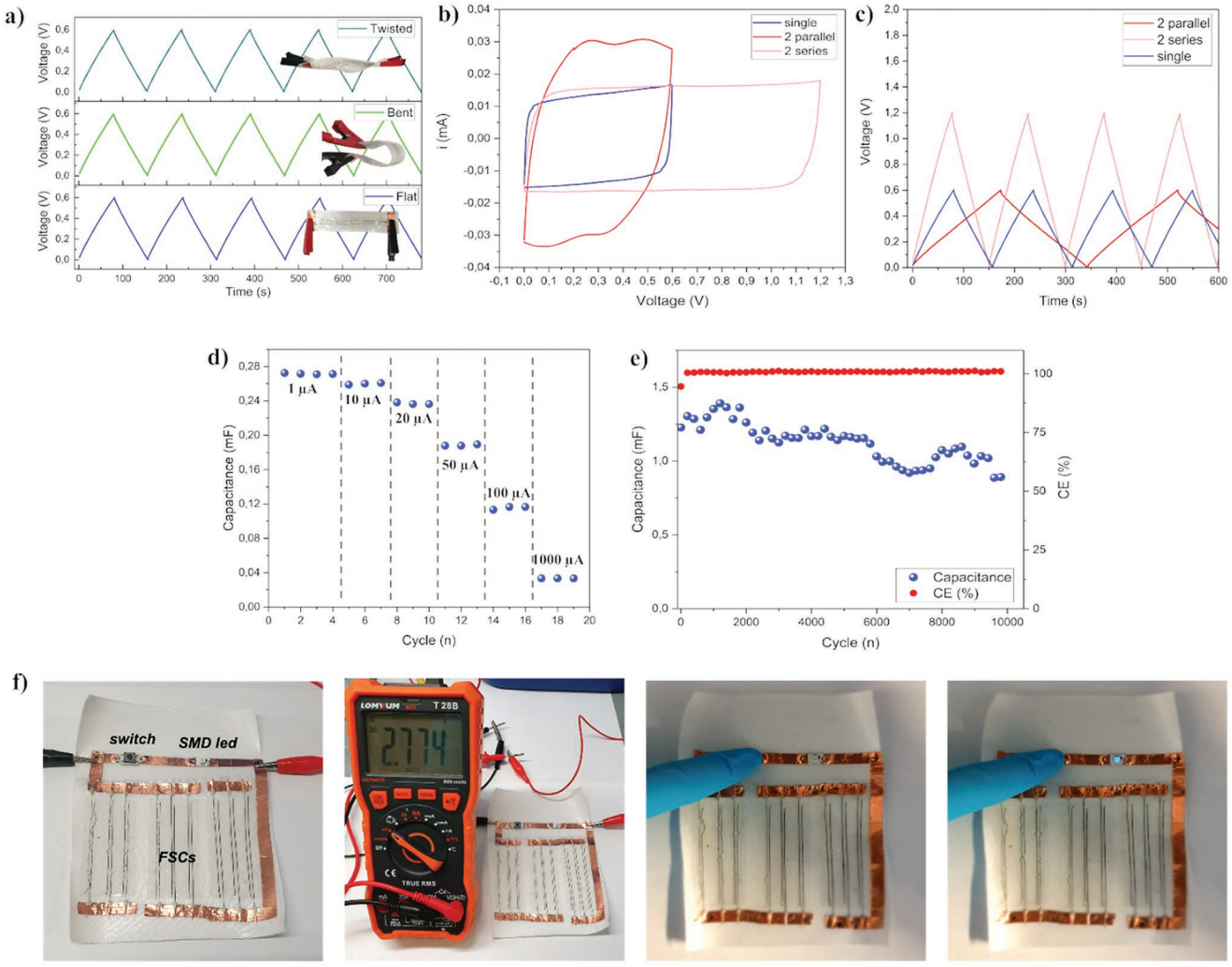

Figure 8. a) Voltage–time profiles of charge/discharge of sewed FSCs at rest (flat), bent, and twisted deformation. The charge/discharge current is 10 µA for a ≈5 cm long PEDOT:PSS@KNF electrode length. b) Cyclic voltammetries at 10 mV s^{-1} for PEDOT:PSS@KNF electrodes with series and parallel connections. c) Charge/discharge profiles for the single FSC, series and parallelly connected FSC. The charge/discharge current is 10 µA for ≈5 cm PEDOT:PSS@KNF electrode length. Rate capability test at different currents for the single FSC (d) and long duration test in (e). In (f), an array of PEDOT:PSS@KNF FSCs was produced by fixing the wire-shaped electrodes with a bi-adhesive tape at the extremities and connecting them to the e-textile circuit.

111 to 819 Ohm (Figure 7c). Moreover, the almost vertical slope of the line in the low frequency region was representative of the good capacitive behavior of the PEDOT:PSS@KNF electrodes. In the rate capability test performed through CVs (Figure 7d), the almost rectangular shape was maintained even at 100 mV s^{-1}. The capacitance data (Figure 7e, detailed values in Table S2, Supporting Information) showed again decreasing capacitance at increasing scan rate but retaining the 60% of the capacitance at the highest scan rate. The capacitance of the sewed symmetric FSC device at an average scan rate (10 mV s^{-1}) was as high as 0.26 mF cm^{-1}, 8.33 mF cm^{-2}, 3.33 F cm^{-3}, and 2 F g^{-1}.

The FSC performances were investigated under different deformations since in real application a textile energy storage device may be subjected to a series of different stimuli. **Figure 8**a shows that the voltage-time profile of our FSC in rest configuration (flat) was identical to the one related to the FSC obtained by bending it several times at 180° and then keeping it bent. The same was done by twisting it. These results confirmed again the remarkable flexibility of the PEDOT:PSS@KNF electrodes. To increase the overall energy output of the FSC device, arrays of series and parallel connections could be produced. Figure 8b highlights that by series connection the overall voltage window can be doubled and by parallel connection the current is increased. By charging/discharging the FSC devices, the voltage profiles (Figure 8c) coherently demonstrates that by parallel and series connection of two PEDOT:PSS@KNF FSCs the discharge time and voltage windows were almost doubled respectively. Small deviations respect to the single FSC device may be ascribed to the hand-made preparation of the devices. In terms of energy output, the energy released during discharge was 6.2 mWh for the single FSC, 12 and 13.5 mWh for the series and parallel connected FSCs respectively, meaning an approximately twofold increase of energy discharged.

The single PEDOT:PSS@KNF symmetrical FSC decreased its linear capacitance from 0.27 to 0.04 mF cm^{-1} when discharged at 1 µA (0.75 mA g^{-1}) and 1000 µA (765 mA g^{-1}),

respectively (Figure 8d). The long-duration test revealed a remarkable capacitance retention (Figure 8e), retaining the 80.5% of the initial capacitance after 10K cycles and average coulombic efficiency of 99.1%. However, the slow capacitance drop may be ascribed to the PEDOT:PSS aging effect, recently investigated and attributed to electrodes inhomogeneous electrical and morphological properties.[67] The energy and power averaged on the 10K cycles and normalized on device length and area (considering as active area only the electrodes surface) are 5.5 μWh cm^{-1}, 177 μWh cm^{-2}, 290 μW cm^{-1}, and 950 μW cm^{-2} (other detailed values are given in Table S3, Supporting Information). Compared to similar works (Table S4, Supporting Information), the surface and volumetric energy and power are much higher meaning that our PEDOT:PSS@KNF fibers are highly performing electrodes for electrochemical capacitors and the proposed synthesis method is a valid alternative to other literature approaches. Finally, an array of three series of three parallelly connected FSCs was produced and integrated into an electrical circuit comprised of a button switch and a blue SMD led (forward voltage ≈2.5 V) (Figure 8f). The aim was a proof-of-concept demonstration of the actual integration of our developed PEDOT:PSS@KNF FSCs in a real e-textile circuit. The FSCs array was charged up to 2.8 V with an external power supply and showed a stable voltage of ≈2.77 V by disconnecting the external potentiostat. After removing all external electrical connections, the blue led could be powered on for several seconds by pressing the electrical switch. Since the charge storage mechanism in our PEDOT:PSS@KNF FSCs is surface-limited (double-layer and surface redox), in principle the overall capacitance of the system could be increased by an accurate morphology control of the fibers aiming to increase the surface-to-length ratio. However, PEDOT:PSS@KNF FSCs were mainly limited in capacitance by the narrow operational potential window. PEDOT:PSS@KNF electrodes loaded with high working potential electrode (typically MnO_2) may overcome the aforementioned limitation and could be subject of future works.

3. Conclusion

Composite fibers of PEDOT:PSS loaded into a Kevlar nanofibers matrix were prepared by a two-step process including wet spinning and immersion of the KNF fibers into the PEDOT:PSS dispersion. The resultant PEDOT:PSS@KNF fibers showed remarkable specific conductivity and good mechanical properties of tensile strength and flexibility that make the PEDOT:PSS@KNF fibers a good candidate for the fabrication of fibrous-shaped 1D capacitors. When used to produce symmetric devices coupled with a semi-solid PVA/H_3PO_4 electrolyte, the textile-FSC showed outstanding capacitance retention under deformation and 80.5% linear capacitance retention after 10K cycles, surpassing similar previous literature works in terms of energy and power density. Moreover, an array of FSCs integrated in a e-textile circuit was able to power on a blue led for several seconds, demonstrating the potential of PEDOT:PSS@KNF fibers and the proposed approach for the fabrication of 1D electrodes for textile capacitors.

4. Experimental Section

Materials: Kevlar 49 fabric was obtained from GoodFellow. Clevios PH1000 (1.0–1.3 wt% PEDOT:PSS) was ordered from Heraeus. DMSO, ethanol, KOH, PVA (M_w 89000–98000, 99+% hydrolyzed), and H_3PO_4 (85 wt%) were obtained from Sigma-Aldrich and used as received.

KNFs Synthesis: KNFs dispersion was achieved following the H_2O deprotonation enhanced method reported by Yang et al. with slight modifications.[31] Briefly, 1 g of Kevlar fabric was cut in pieces and added to a 15.5 g L^{-1} KOH solution in DMSO:H_2O (25:1 v/v). The 1.5 wt% KNFs dispersion was obtained after 24 h of continuous stirring.

Wet Spinning of KNF Fibers and PEDOT:PSS Infiltration: The stable KNFs dispersion was loaded in a 10 mL syringe equipped with a 21G needle, and the KNFs dope was extruded at 0.5 mL min^{-1} into a rotating coagulation bath of EtOH/H_2O/DMSO (3:1:0.1 v/v). The rotation of the coagulation bath was fixed at 25 rpm to have a ≈1.1 draw ratio. The gel-state fibers were transferred to a fresh coagulation bath for several hours, then soaked for 12 h in the PH1000 dispersion diluted at 0.5 wt% with a DMSO/H_2O solution (5% v/v DMSO). Finally the PEDOT:PSS@KNF fibers were collected on a spool and dried at 80 °C overnight. The pure KNF fibers were produced in the same way without the PEDOT:PSS soaking step.

Characterization: Electrode morphology and composition were investigated with scanning electron microscopy (SEM, Zeiss EVO 50 EP) and energy dispersive spectroscopy (EDS, Oxford instruments INCA x-sight detector) operating at 20 kV. AFM measurement was performed in contact mode on a sample prepared by casting a diluted KNF dispersion (<0.1 wt%) on a Si wafer substrate and evaporating DMSO at 100 °C in vacuum. The chemical analyses were performed by Raman spectroscopy (Horiba Jobin Yvon LabRAM HR800 Raman spectrometer) with a 532 nm excitation laser and 25 mW focused by a 50× magnification objective. Microstructure was investigated through X-ray diffraction (Philips model PW1830, Kα1Cu = 1.54058 Å). The mechanical tests were performed with a tensile strength tester (Anton Paar MCR702), at stretching speed of 5 mm min^{-1} and sample length of ≈1.5 cm. Electrical conductivity was measured approximating the fibers to conductive wires and performing cyclic voltammetry between 2 and −2 V at 10 mV s^{-1}. The electrical conductivity (σ, S cm^{-1}) was calculated as $\sigma = L/R \times A$ with R (Ω) measured as the slope of the I–V curve of the CV, L (cm) as the sample length, and A (cm^2) as the cross-section area $A = \pi D^2/4$.

Electrochemical Characterization: The capacitance of the single PEDOT:PSS@KNF fiber was evaluated by cyclic voltammetry using a Squidstat Prime potentiostat (Admiral Instrument) in a 1 M H_3PO_4 solution with Ag/AgCl reference electrode and Pt wire as counter electrode. The FSC semi-solid-state symmetrical devices were obtained by placing adjacently at ≈1 mm the PEDOT:PSS@KNF and pouring a H_3PO_4/PVA gel electrolyte. The devices were then left for several hours at room temperature to remove excess water. EIS measurements were performed in the frequency range 100 kHz–100 mHz with an oscillation amplitude of 10 mV at the open-circuit potential. The specific capacitance, energy density, and power density of all FSCs were calculated from both cyclic voltammetries and galvanostatic discharge data. The capacitance (F) of FSC was extracted from cyclic voltammetry plot according to the following equation $C = \frac{\int I dV}{\nu^* \Delta V}$, where I (mA) is the current, ΔV (V) is the voltage window, and ν is the scan rate (mV s^{-1}). Charge and discharge galvanostatic cycles were performed employing a NEWARE battery tester. The energy and power were calculated according to the equations $E = \frac{1}{2}CV^2$ and $P = \frac{E}{t}$, respectively.[25,68,69]

Supporting Information

Supporting Information is available from the Wiley Online Library or from the author.

Acknowledgements

The authors thank Lorenzo Bonetti and Luigi De Nardo for the mechanical tests.

Open Access Funding provided by Politecnico di Milano within the CRUI-CARE Agreement.

Conflict of Interest

The authors declare no conflict of interest.

Data Availability Statement

The data that support the findings of this study are available from the corresponding author upon reasonable request.

Keywords

capacitors, energy storage, e-textiles, Kevlar nanofibers, PEDOT:PSS, wet-spinning

Received: March 7, 2022
Revised: May 20, 2022
Published online:

[1] J. S. Heo, J. Eom, Y.-H. Kim, S. K. Park, *Small* **2018**, *14*, 1703034.
[2] T. Hughes-Riley, T. Dias, C. Cork, *Fibers* **2018**, *6*, 34.
[3] T. M. Fernández-Caramés, P. Fraga-Lamas, *Electronics* **2018**, *7*, 405.
[4] I. Ibanez-Labiano, M. S. Ergoktas, C. Kocabas, A. Toomey, A. Alomainy, E. Ozden-Yenigun, *Appl. Mater. Today* **2020**, *20*, 100727.
[5] E. Ismar, S. Kurşun Bahadir, F. Kalaoglu, V. Koncar, *Global Challenges* **2020**, *4*, 1900092.
[6] M. Wagih, Y. Wei, A. Komolafe, R. Torah, S. Beeby, *Sensors* **2020**, *20*, 3435.
[7] X. Shi, Y. Zuo, P. Zhai, J. Shen, Y. Yang, Z. Gao, M. Liao, J. Wu, J. Wang, X. Xu, Q. Tong, B. Zhang, B. Wang, X. Sun, L. Zhang, Q. Pei, D. Jin, P. Chen, H. Peng, *Nature* **2021**, *591*, 240.
[8] H.-J. Park, S. Kim, J. H. Lee, H. T. Kim, W. Seung, Y. Son, T. Y. Kim, U. Khan, N.-M. Park, S.-W. Kim, *ACS Appl. Mater. Interfaces* **2019**, *11*, 5200.
[9] G. M. N. Islam, A. Ali, S. Collie, *Cellulose* **2020**, *27*, 6103.
[10] S. Seyedin, P. Zhang, M. Naebe, S. Qin, J. Chen, X. Wang, J. M. Razal, *Mater. Horiz.* **2019**, *6*, 219.
[11] S. W. Lee, H. G. Jung, I. Kim, D. Lee, W. Kim, S. H. Kim, J.-H. Lee, J. Park, J. H. Lee, G. Lee, D. S. Yoon, *ACS Appl. Mater. Interfaces* **2020**, *12*, 46629.
[12] J. Luo, S. Gao, H. Luo, L. Wang, X. Huang, Z. Guo, X. Lai, L. Lin, R. K. Y. Li, J. Gao, *Chem. Eng. J.* **2021**, *406*, 126898.
[13] D.-H. Kim, J.-H. Cha, J. Y. Lim, J. Bae, W. Lee, K. R. Yoon, C. Kim, J.-S. Jang, W. Hwang, I.-D. Kim, *ACS Nano* **2020**, *14*, 16907.
[14] S. Nasiri, M. R. Khosravani, *Sens. Actuators, A* **2020**, *312*, 112105.
[15] W. Fan, Q. He, K. Meng, X. Tan, Z. Zhou, G. Zhang, J. Yang, Z. L. Wang, *Sci. Adv.* **2020**, *6*, eaay2840.
[16] F. Mo, G. Liang, Z. Huang, H. Li, D. Wang, C. Zhi, *Adv. Mater.* **2020**, *32*, 1902151.
[17] S. Chen, W. Ma, Y. Cheng, Z. Weng, B. Sun, L. Wang, W. Chen, F. Li, M. Zhu, H.-M. Cheng, *Nano Energy* **2015**, *15*, 642.
[18] Z. Yang, Y. Jia, Y. Niu, Y. Zhang, C. Zhang, P. Li, M. Zhu, Q. Li, *J. Energy Chem.* **2020**, *51*, 434.
[19] N. He, Q. Pan, Y. Liu, W. Gao, *ACS Appl. Mater. Interfaces* **2017**, *9*, 24568.
[20] S. H. Aboutalebi, R. Jalili, D. Esrafilzadeh, M. Salari, Z. Gholamvand, S. Aminorroaya Yamini, K. Konstantinov, R. L. Shepherd, J. Chen, S. E. Moulton, P. C. Innis, A. I. Minett, J. M. Razal, G. G. Wallace, *ACS Nano* **2014**, *8*, 2456.
[21] Z. Lu, J. Foroughi, C. Wang, H. Long, G. G. Wallace, *Adv. Energy Mater.* **2018**, *8*, 1702047.
[22] Y. Shang, C. Wang, X. He, J. Li, Q. Peng, E. Shi, R. Wang, S. Du, A. Cao, Y. Li, *Nano Energy* **2015**, *12*, 401.
[23] J. Di, X. Zhang, Z. Yong, Y. Zhang, D. Li, R. Li, Q. Li, *Adv. Mater.* **2016**, *28*, 10529.
[24] N. Behabtu, C. C. Young, D. E. Tsentalovich, O. Kleinerman, X. Wang, A. W. K. Ma, E. A. Bengio, R. F. ter Waarbeek, J. J. de Jong, R. E. Hoogerwerf, S. B. Fairchild, J. B. Ferguson, B. Maruyama, J. Kono, Y. Talmon, Y. Cohen, M. J. Otto, M. Pasquali, *Science* **2013**, *339*, 182.
[25] Z. Wang, J. Cheng, Q. Guan, H. Huang, Y. Li, J. Zhou, W. Ni, B. Wang, S. He, H. Peng, *Nano Energy* **2018**, *45*, 210.
[26] J. Zhang, S. Seyedin, S. Qin, P. A. Lynch, Z. Wang, W. Yang, X. Wang, J. M. Razal, *J. Mater. Chem. A* **2019**, *7*, 6401.
[27] D. Yuan, B. Li, J. Cheng, Q. Guan, Z. Wang, W. Ni, C. Li, H. Liu, B. Wang, *J. Mater. Chem. A* **2016**, *4*, 11616.
[28] W. Eom, H. Shin, R. B. Ambade, S. H. Lee, K. H. Lee, D. J. Kang, T. H. Han, *Nat. Commun.* **2020**, *11*, 2825.
[29] A. Levitt, J. Zhang, G. Dion, Y. Gogotsi, J. M. Razal, *Adv. Funct. Mater.* **2020**, *30*, 2000739.
[30] M. Yang, K. Cao, L. Sui, Y. Qi, J. Zhu, A. Waas, E. M. Arruda, J. Kieffer, M. D. Thouless, N. A. Kotov, *ACS Nano* **2011**, *5*, 6945.
[31] B. Yang, L. Wang, M. Zhang, J. Luo, X. Ding, *ACS Nano* **2019**, *13*, 7886.
[32] B. Zhang, W. Wang, M. Tian, N. Ning, L. Zhang, *Eur. Polym. J.* **2020**, *139*, 109996.
[33] J. Fan, J. Wang, Z. Shi, S. Yu, J. Yin, *Mater. Chem. Phys.* **2013**, *141*, 861.
[34] Y. Zhao, X. Li, J. Shen, C. Gao, B. V. der Bruggen, *J. Mater. Chem. A* **2020**, *8*, 7548.
[35] S. Yuan, J. Swartenbroekx, Y. Li, J. Zhu, F. Ceyssens, R. Zhang, A. Volodine, J. Li, P. Van Puyvelde, B. Van der Bruggen, *J. Membr. Sci.* **2019**, *573*, 612.
[36] L. Liu, Z. Li, Q. Che, *ACS Appl. Nano Mater.* **2019**, *2*, 2160.
[37] Z. Zhang, S. Yang, P. Zhang, J. Zhang, G. Chen, X. Feng, *Nat. Commun.* **2019**, *10*, 2920.
[38] Z. Liu, J. Lyu, D. Fang, X. Zhang, *ACS Nano* **2019**, *13*, 5703.
[39] J. Lyu, Z. Liu, X. Wu, G. Li, D. Fang, X. Zhang, *ACS Nano* **2019**, *13*, 11392.
[40] B. Yang, L. Wang, M. Zhang, W. Li, Q. Zhou, L. Zhong, *J. Mater. Chem. A* **2021**, *9*, 12923.
[41] L. Liu, J. Lyu, J. Mo, H. Yan, L. Xu, P. Peng, J. Li, B. Jiang, L. Chu, M. Li, *Nano Energy* **2020**, *69*, 104398.
[42] W. Cao, L. Yang, X. Qi, Y. Hou, J. Zhu, M. Yang, *Adv. Funct. Mater.* **2017**, *27*, 1701061.
[43] A. Wang, X. Zhang, F. Chen, Q. Fu, *Carbon* **2021**, *179*, 655.
[44] B. Yang, L. Wang, M. Zhang, J. Luo, Z. Lu, X. Ding, *Adv. Funct. Mater.* **2020**, *30*, 2000186.
[45] H. Shi, C. Liu, Q. Jiang, J. Xu, *Adv. Electron. Mater.* **2015**, *1*, 1500017.
[46] W. Meng, R. Ge, Z. Li, J. Tong, T. Liu, Q. Zhao, S. Xiong, F. Jiang, L. Mao, Y. Zhou, *ACS Appl. Mater. Interfaces* **2015**, *7*, 14089.
[47] Y. Xia, J. Ouyang, *J. Mater. Chem.* **2011**, *21*, 4927.
[48] I. Lee, G. W. Kim, M. Yang, T.-S. Kim, *ACS Appl. Mater. Interfaces* **2016**, *8*, 302.
[49] S. Zhang, P. Kumar, A. S. Nouas, L. Fontaine, H. Tang, F. Cicoira, *APL Mater.* **2015**, *3*, 014911.
[50] E. Hosseini, V. O. Kollath, K. Karan, *J. Mater. Chem. C* **2020**, *8*, 3982.
[51] J. E. McCarthy, C. A. Hanley, L. J. Brennan, V. G. Lambertini, Y. K. Gun'ko, *J. Mater. Chem. C* **2013**, *2*, 764.

[52] Q. Gao, M. Wang, X. Kang, C. Zhu, M. Ge, *Compos. Comm.* **2020**, *17*, 134.
[53] X. Wang, G. Feng, M. Ge, *J. Mater. Sci.* **2017**, *52*, 6917.
[54] X. Li, Y. Liu, Z. Shi, C. Li, G. Chen, *RSC Adv.* **2014**, *4*, 40385.
[55] J. Zhou, E. Q. Li, R. Li, X. Xu, I. A. Ventura, A. Moussawi, D. H. Anjum, M. N. Hedhili, D.-M. Smilgies, G. Lubineau, S. T. Thoroddsen, *J. Mater. Chem. C* **2015**, *3*, 2528.
[56] Y. Kim, A. Lund, H. Noh, A. I. Hofmann, M. Craighero, S. Darabi, S. Zokaei, J. I. Park, M.-H. Yoon, C. Müller, *Macromol. Mater. Eng.* **2020**, *305*, 1900749.
[57] Y. Chen, J. Meng, Y. Xu, Y. Li, Q. Zhang, C. Hou, H. Sun, G. Wang, H. Wang, *Adv. Electron. Mater.* **2021**, *7*, 2100231.
[58] R. Sarabia-Riquelme, R. Andrews, J. E. Anthony, M. C. Weisenberger, *J. Mater. Chem. C* **2020**, *8*, 11618.
[59] N. Wen, Z. Fan, S. Yang, Y. Zhao, T. Cong, S. Xu, H. Zhang, J. Wang, H. Huang, C. Li, L. Pan, *Nano Energy* **2020**, *78*, 105361.
[60] D. Feng, P. Wang, M. Wang, C. Zhu, Q. Gao, M. Shen, *Fibers Polym.* **2021**, *22*, 1491.
[61] L. Wang, M. Zhang, B. Yang, J. Tan, *ACS Appl. Mater. Interfaces* **2021**, *13*, 41933.
[62] A. Zykwinska, W. Domagala, B. Pilawa, M. Lapkowski, *Electrochim. Acta* **2005**, *50*, 1625.
[63] M. Demelas, E. Scavetta, L. Basiricò, R. Rogani, A. Bonfiglio, *Appl. Phys. Lett.* **2013**, *102*, 193301.
[64] A. V. Volkov, K. Wijeratne, E. Mitraka, U. Ail, D. Zhao, K. Tybrandt, J. W. Andreasen, M. Berggren, X. Crispin, I. V. Zozoulenko, *Adv. Funct. Mater.* **2017**, *27*, 1700329.
[65] Y. Li, G. Ren, Z. Zhang, C. Teng, Y. Wu, X. Lu, Y. Zhu, L. Jiang, *J. Mater. Chem. A* **2016**, *4*, 17324.
[66] L. Manjakkal, A. Pullanchiyodan, N. Yogeswaran, E. S. Hosseini, R. Dahiya, *Adv. Mater.* **2020**, *32*, 1907254.
[67] H. Ur Rehman, A. Shuja, M. Ali, I. Murtaza, H. Meng, *J. Energy Storage* **2020**, *28*, 101243.
[68] H. Fang, L. Yuan, G. Liang, A. Gu, *Electrochim. Acta* **2018**, *284*, 149.
[69] S. Cai, T. Huang, H. Chen, M. Salman, K. Gopalsamy, C. Gao, *J. Mater. Chem. A* **2017**, *5*, 22489.